Structure of the fully hydrated gel phase of dipalmitoylphosphatidylcholine

M. C. Wiener,* R. M. Suter,* and J. F. Nagle*‡
Departments of *Physics and ‡Biological Sciences, Carnegie Mellon University, Pittsburgh, Pennsylvania 15213

ABSTRACT X-ray diffraction intensities for lamellar repeats, h = 1 to 7, and wide-angle x-ray scattering were measured for the gel phase of fully hydrated dipalmitoylphosphatidylcholine. A hybrid model, which represents the electron density along the lamellar repeat direction as a continuous function composed of constant strips and superimposed Gaussians, is defined. The data were used to determine the best parameters in hybrid models and also in the older strip models. The most successful results were obtained when the density of the methylene region was constrained to the value obtained from the wide-angle scattering. Further analysis utilized the lipid volume obtained from absolute specific volume measurements. Together with the fundamental relations derived in the previous paper, the electron density modeling yielded the headgroup volume (340 ± 10 Å^3) and the methylene volume (25.3 ± 0.2 Å^3). The results were in agreement whether the hybrid model or the strip model was used and whether our data or the data of Torbet and Wilkins were used. Additional structural results, such as the area (45.9 ± 2.0 Å^2) and the number of waters of hydration per lipid (10.6 ± 2.0), required one additional piece of information, which we took to be the tilt angle θ, which is 30 ± 3° from other experiments in the literature. Absolute electron density profiles, which clearly indicate two features in the headgroup region, are presented. The analysis yielded an accurate value of $F(0)$, which contributes to the continuous scattering transform $F(X)$, which is also given.

INTRODUCTION

Many studies have been performed to elucidate the structure of lipid bilayers and much progress has been made (1–18). There has been a tendency for the different studies to focus upon different structural quantities and to use different methods. Not surprisingly, inconsistencies have become apparent when the results are compared. Some of these inconsistencies have been discussed in a previous paper (19), which systematically sets forth many relations between different quantities. One purpose of this paper is to develop a unified method of analysis that can use a greater variety of data in a consistent way and that can indicate where the inconsistencies are. Another purpose is to establish reliable structural results for the benchmark lipid dipalmitoylphosphatidylcholine (DPPC).

Low-angle diffraction from the stacking of bilayers in multilamellar vesicles provides several kinds of average structural information about the bilayer. The most direct result is the distance D from the center of one bilayer to the next in the stack. This distance D increases with the amount of water added until it becomes constant when water is added in excess. Determining the amount of water at the point of D becoming constant yields the number of waters per lipid, n_W, for the fully hydrated system (1–3, 5). The quantity n_W is related to the area A of each lipid in the plane of the membrane by

$$A = 2(V_L + n_W V_W)/D, \quad (1)$$

where V_W is the molecular volume of water and V_L is the volume of the lipid molecule in a fully hydrated system, which is obtained from specific volume measurements (20, 21). Though simpler in appearance, Eq. 1 is fully equivalent to the formula introduced many years ago by Luzzati (6). This relation has been employed frequently to obtain A from V_L, n_W, and D (1–3). However, the estimates of A are subject to fluctuations in the determination of n_W, which are considerable. For the G phase of DPPC, n_W has been given as 9 (7), 13.6 (3), 17.5 (2), and 19 (1), which lead to values of A between 44.4 and 53.6 Å^2 using Eq. 1 and measurements of V_L and D. Values of A given in the literature range from 43.8 (8) to 52.3 (2) Å^2. Since the minimal value of A that corresponds to very close packing of crystalline chains is ~39 Å^2, the relative uncertainties in the A determination are large.

In addition to determining D, low-angle diffraction data also yield relative intensities, $I(h)$, of the different orders of diffraction from which, with careful consideration of the phase problem (9), the first five to ten relative structure factors, $F(h)$, have been determined and truncated Fourier series representations of relative electron

Dr. Wiener's present address is Department of Physiology and Biophysics, University of California at Irvine, Irvine, CA 92717.

density profiles have been plotted (9–11). These profiles indicate that there are electron-sparse terminal methyl regions in the center of the bilayer and they give accurate estimates for the locations of the peaks in electron density of the headgroups. However, the Fourier profiles have not yielded any other direct structural information. Strip models for electron density profiles have been employed (12) to estimate the boundary between the headgroups and the chain region, i.e., the thickness of the hydrocarbon chain region, which will be designated $2D_C$ for the full bilayer. A strongly contrasting Gaussian model was introduced by Mitsui (8), who modeled an asymmetric bilayer system as two different Gaussian functions, each corresponding to a headgroup. In this paper, a new electron density model, the hybrid model, which combines aspects of both the strip and Gaussian models, will be presented. Also, there are additional relations between electron density models and other structural information that have only recently been developed (22). One of the purposes of this paper is to illustrate the use of these relations for the analysis of the gel phase of DPPC.

A different way to obtain structural information about lipid bilayers is to analyze the wide-angle diffraction between hydrocarbon chains. In chain-ordered phases, such as the gel phase of DPPC, it has usually been assumed (1, 4, 13) that the hydrocarbon chains are packed in an orthorhombic array, which is nearly hexagonal when projected onto a plane perpendicular to the chains. One study (8) allowed for an oblique lattice, but the oblique angle was close enough to orthorhombic that the use of the orthorhombic formulae makes little difference. The plane perpendicular to the chains is generally tilted by an angle θ from the plane of the bilayer, so not all the diffraction maxima fall on the equator for oriented samples. The wide-angle diffraction from unoriented samples of the gel phase of DPPC consists of a sharp peak, which is indexed as the (2, 0) reflection from the nearly hexagonal chain packing, and a broader shoulder, which is often indexed as the (1, ±1) reflections from the chain packing. From this assignment the cross-sectional area A_c of the chains in the plane perpendicular to the chains can be determined from the positions of the two reflections, but this does not determine the area A of each lipid (each with two chains) in the plane of the membrane, which is related only by

$$A = 2A_c \cos\theta. \quad (2)$$

From A_c the electron density of the methylene chains is easily determined using

$$\rho^*_{CH_2} = n^*_{CH_2}/(1.27\,A_c), \quad (3)$$

where $n^*_{CH_2}$ is the number of electrons per CH_2 and the projected separation of methylenes along an all-*trans* chain is 1.27 Å. Values of $\rho^*_{CH_2}$ for the gel phase of DPPC at room temperature that have been given or that can be deduced from the literature are 0.323 (1), 0.317 (10), 0.315 (8), and 0.319 (4) e/Å^3. In oriented samples, wide-angle chain-packing reflections should appear on the Bragg rods perpendicular to the plane of the bilayer. The particular interpretation of the pattern from unoriented samples corresponds to the (2, 0) reflection appearing on the equator and the (1, ±1) reflections appearing at an angle from the equator that is closely related to θ. Levine (13) measured this angle for the (1, ±1) reflections in oriented samples and obtained a value of $\theta = 28°$.

Finally, we should mention that there are a number of eclectic, but often quite powerful, methods for obtaining structural information about bilayers that should not be ignored. One method relies on measurements in two similar lipids. For example, McIntosh (10) compared the gel phase of DPPC with the gel phase of diphosphatidylethanolamine (DPPE), since DPPE has a simpler wide-angle pattern attributed to the chains being untilted. Consistent with this the Fourier electron density profiles yielded a smaller headgroup–headgroup separation in DPPC. Assuming that this smaller distance for DPPC is due entirely to tilt in the chains and not due to differences in headgroup orientations, a tilt angle $\theta = 31°$ can be obtained. This value is in good agreement with Levine's result (13) and also with the result $\theta = 27°$ that can be deduced by comparing the positions of the C4 and C14 methylenes obtained from low-angle neutron diffraction for selectively deuterated/protonated methylenes (14). Another method obtains structural information about one phase of a lipid and then relates it to another phase. For example, we obtained a value of the volume of the headgroup V_H for DPPC in the subgel, fully hydrated C phase for which there is additional diffraction information (19). Since the gel phase is also fully hydrated and since the water would be expected to fill any voids in both phases (20, 21), V_H should be the same as in the C phase. Another example that uses information about one phase to determine information about another phase has recently been given by McIntosh and Simon (15, 19).

MATERIALS AND METHODS

DPPC was purchased from Avanti Polar Lipids, Inc. (Birmingham, AL) and used as received. Lipid purity was judged to be excellent based on calorimetric and dilatometric half-widths of 0.1°C for the main transition. All samples were fully hydrated with 50% or more water by weight. Hydrated samples were taken five times through the following thermomechanical cycle: suspension in a water bath 10–15°C above the main phase transition temperature for several minutes followed by brief vortexing, followed by suspension in an ice-water slurry for several minutes, followed by brief vortexing. The hydrated lipid was then loaded into 1-mm glass capillary tubes and flame-sealed.

An Elliott GX21 rotating-anode x-ray generator (Enraf-Nonius

Service Corp., Bohemia, NY) was used with graphite monochromator and Bicron NaI scintillator-photomultiplier detector (Blake Industries, Inc., Scotch Plains, NJ) to record the diffraction patterns from the samples. The sample was mounted on a Huber 511.1 four circle goniometer (Blake Industries, Inc.) which provided precision angular control. The intrinsic resolution width of diffraction peaks with this configuration is 0.01 $Å^{-1}$. All experiments were performed at $T = 20 \pm 2°C$. The integrated intensities of the low-angle lamellar reflections were obtained by several methods of computer integration. The differences between methods involved different choices of baselines. Baseline curves were constructed with a computer graphics program or obtained from the scattering data of capillary tubes containing water and no lipid. Also, the integrated intensities were obtained either by numerical integration or by fitting the diffraction peaks with Gaussian lineshapes. The differences from these various integration procedures were smaller than the variations from one sample to another. The integrated intensities were multiplied by the Lorentz-polarization correction factor, which is $\sim h^2$, to yield $I(h)$. To obtain structure factors, $F(h)$, the square root of $I(h)$ was taken and the phases ($\pm$) of Torbet and Wilkins (9) were used.

The strip model represents the electron density $\rho^*(x)$ versus distance x from the center of the bilayer as a sequence of strips, each with a constant density ρ_i and width x_i. Two different strip models were utilized in this paper. A four-strip model, to be called the 4S model, represents each of the four parts of the bilayer (terminal methyl, methylene, headgroup, and interlamellar water) as a single strip; a five-strip model, to be called the 5S model, represents the headgroup by two strips instead of one strip as in the 4S model. Each strip has a width and electron density, but the sum of strip widths must add to $D/2$, so the model is specified by $2N - 1$ parameters. The structure factors $F(h)$ have a simple analytic form (16).

The hybrid models introduced and developed in this paper contain features of both the strip model and the Gaussian model introduced by Mitsui (8). The interlamellar water region and the methylene regions of the bilayer are first approximated as constant density regions (strips). In the headgroup region a gap proportional to the width of the headgroup is left between these strips which is bridged by a bridging function that was chosen to be half the period of a sine function with amplitude equal to the difference in electron densities of the water and methylene regions. (See right-hand side of Fig. 1.) The headgroup regions and the terminal methyl region are represented by Gaussians which are superimposed on the bridged strip functions. Hybrid models therefore represent the electron density $\rho^*(x)$ as a function that is continuous and has a continuous first derivative. Two specific hybrid models were considered in this study. For the 1G hybrid model each of the two headgroups is represented by one Gaussian function. For the 2G hybrid model each of the two headgroups is represented by two Gaussians. A 2G hybrid model electron density profile is depicted in Fig. 1. The number of parameters required to specify the hybrid models is the sum of three for each headgroup Gaussian (position X_{Hi}, amplitude C_{Hi}, and width σ_{Hi}), two for the terminal methyl Gaussian (amplitude C_{Hi} and width σ_{Hi}) and one each for the electron density of the fluid region (ρ^*_W) and the methylene region ($\rho^*_{CH_2}$). The constant methylene baseline extends from 0 to $X_{H1} - \sigma_{H1}$ and the constant water baseline extends from $X_{H2} + \sigma_{H2}$ to $D/2$. The mathematical definitions of the hybrid models and the functional form of the structure factors $F(h)$ are given in detail (23).

Nonlinear least-squares fitting of strip and hybrid model electron density profiles to the measured low-angle intensity data $I(h)$ was performed. The best fit to the data is defined to be that given by the electron density model parameter set $\mathbf{p}$ that minimizes the sum of the square of the residuals, $R^2(h; \mathbf{p})$:

$$R^2(h; \mathbf{p}) = \sum_{h=1}^{H} w(h)\,[I(h; \mathbf{obs}) - I(h; \mathbf{p})]^2, \qquad (4)$$

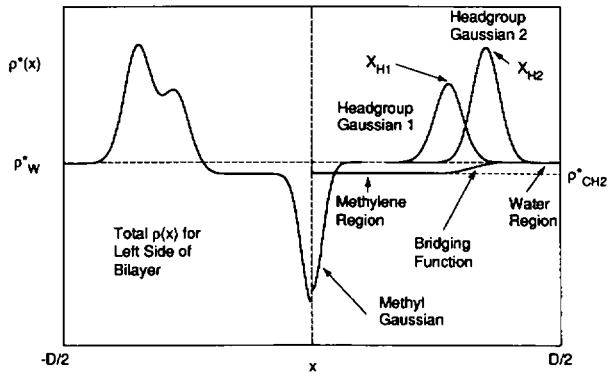

FIGURE 1 Electron density profile $\rho^*(x)$ as a function of distance x from the center of the bilayer for a 2G hybrid model is depicted on the left-hand side for half a bilayer. The right side depicts the constituent parts of the profile.

where the sum is from 1 to H, the highest lamellar diffraction order observed. The weighting function $w(h)$ is equal to $1/\sigma_h^2$, where σ_h are the experimental uncertainties for the intensities. Fits to the data of Torbet and Wilkins (9) used equal weights $w(h)$ for all h.

RESULTS

Lamellar low-angle diffraction from the gel phase of DPPC was recorded and orders $h = 1$ to 5 and the 7th order were observed as shown in Fig. 2 for a representative experiment. The peak widths are the resolution width

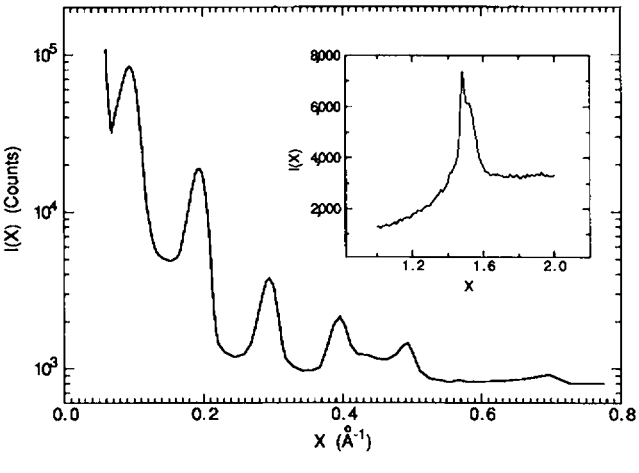

FIGURE 2 Relative scattering intensity $I(X)$ versus reciprocal space distance X of G phase DPPC at 20 ± 2°C. The body of the figure shows the seven orders of low-angle lamellar diffraction recorded in a typical experiment; the inset shows the wide-angle diffraction pattern. Notice the use of a logarithmic scale for the body of the figure which exaggerates the apparent width of the peaks and the baseline features but emphasizes the dynamic range of the data.

0.01 $Å^{-1}$ of the diffractometer configuration. A limited amount of data was also taken using a silicon monochromator and the true width of the $h = 1$ peak is 0.005 $Å^{-1}$.

Our structure factors with errors are given in column 2 of Table 1 along with those obtained from Torbet and Wilkins (9) (designated TW) and McIntosh and Simon (11) (designated MS). Each data set is normalized by the factor α (17), given by

$$\alpha^{-2} = \frac{D_0}{D} \sum_{h=1}^{H} |F(h)|^2. \quad (5)$$

The reference D-spacing D_0 is chosen to be 63.7 Å, our result for the bilayer repeat. The sum in Eq. 8 was restricted to $H = 5$ so as to treat all data sets uniformly. The different data sets are consistent within the estimated experimental error. Although we did not observe the $h = 8$ order, we estimate that its absolute value is <0.1. For some of the subsequent calculations $F(8)$ will be taken to be zero, which is within experimental error of the value found by TW (9). The values of $F(0)$ given in Table 1 are not obtained directly from the experiments but will be determined subsequently.

Diffraction in the wide-angle region is shown in the inset of Fig. 2. It consists of a sharp peak at 4.23 ± 0.02 Å and a broader shoulder at 4.12 ± 0.02 Å. Indexing these to the [2, 0] and [1, ±1] reflections, respectively, yields a chain packing orthorhombic unit cell with $a = 8.46 \pm 0.04$ Å and $b = 4.71 \pm 0.03$ Å containing two hydrocarbon chains, each of which has $A_C = 19.9 \pm 0.2$ $Å^2$ and a methylene density $\rho^*_{CH_2} = 0.317 \pm 0.003$ $e/Å^3$, in reasonable agreement with the literature values mentioned in the Introduction.

TABLE 1 Measured and calculated relative (normalized) structure factors $F(h)$, with experimental uncertainties in parentheses, for the G phase of DPPC (T = 20°C)

	Data			Calculated			
h	This paper	MS (11)	TW (9)	1G	2G	5S	2G (TW)
0	0.388 (0.014)	0.25	0.86	0.444	0.400	0.392	0.373
1	−0.61 (0.05)	−0.68	−0.62	−0.71	−0.66	−0.65	−0.61
2	−0.57 (0.02)	−0.57	−0.60	−0.54	−0.56	−0.56	−0.59
3	+0.36 (0.03)	+0.33	+0.33	+0.37	+0.36	+0.36	+0.34
4	−0.33 (0.03)	−0.26	−0.28	−0.31	−0.31	−0.32	−0.28
5	−0.24 (0.02)	−0.22	−0.28	−0.26	−0.24	−0.24	−0.31
6	0.00 (0.01)	0.00	−0.01	0.00	0.00	−0.00	−0.03
7	−0.17 (0.02)	—	−0.20	−0.12	−0.17	−0.17	−0.22
8	~0.0 (0.1)	—	−0.03	−0.09	0.00	0.00	−0.02
9	—	—	−0.12	−0.05	−0.08	−0.08	−0.11
10	—	—	−0.21	−0.05	−0.07	0.03	−0.19
D	63.7 (0.3)	63.6	64	—	—	—	—
K	—	—	—	2.46	2.72	2.79	2.92

The absolute structure factors are given by $KF(h)$ where our best estimates of K (in $e/Å^3$) are given in the last line.

Hybrid models and strip models were fit to the structure factors $F(h)$ shown in Table 1 as well as to the squares of the structure factors, $I(h) = |F(h)|^2$, with the weights in Eq. 8 consistently assigned for the intensity data. It made virtually no difference whether the fitting was to the structure factors, which include the phases assigned by Torbet and Wilkins (9), or whether the fit was to the intensities, which include no phase information. This simply means that the initial electron density models were chosen sufficiently close to the final ones that the subsequent refinement involved in the fitting was not sensitive to the phases. Some models were fit to the data of Torbet and Wilkins (9) and will be denoted by (TW), e.g., 2G (TW) hybrid model; all other models were fit to the data obtained in this study.

The first set of fits will be called unconstrained fits because all the parameters in the models are allowed to vary to obtain the best fit, except the fluid electron density ρ^*_W, which is replaced by zero in the minus fluid characterization (18) for which $F(0)$ is calculated. The results were unsatisfactory in predicting the value of $\rho^*_{CH_2}$. In particular, different models and different sets of data gave values of $\rho^*_{CH_2}$ whose differences were of order 0.02, which is more than six times the experimental error seen in the wide-angle diffraction. To investigate this negative result further, some purely model calculations were performed. These calculations utilized a known electron density profile and its Fourier intensities $I(h)$ for $h < H$. Electron density models with constrained values of the methylene electron density ρ_{CH_2} were then fit to these "data." The result was consistent with the results mentioned above for the real data, namely, variations of ρ_{CH_2} that were six times the experimental uncertainty from the wide-angle measurements gave results for the structure factors that were within experimental error. These results mean that $\rho^*_{CH_2}$ is not well-determined by electron density models obtained from low-angle intensity data compared to the precision obtained from using the wide-angle diffraction data and making the standard assumption of orthorhombic chain packing. This outcome is a result of the small difference in electron density between the methylene region of the bilayer and the water in which the lipid is dispersed; the methylene region thus makes a rather small contribution to the low-angle lamellar diffraction. This minor influence on the intensities leads to the insensitivity

of the unconstrained models in the determination of $\rho^*_{CH_2}$. It should be noted that this fundamental problem of low contrast in x-ray diffraction of phospholipids is eliminated in neutron diffraction studies, where the large difference in scattering lengths of the proton and deuteron can be utilized.

Because of the results in the preceding paragraphs the principal fits to the low-angle diffraction data were constrained fits in which $\rho^*_{CH_2}$ was chosen to be in the range determined by wide-angle results. The fitted values of $F(h)$ are shown in the last four columns of Table 1 for $\rho^*_{CH_2} = 0.317$ e/Å^3. These values of $F(h)$ obtained from the constrained fits are reasonably consistent with the measured values when experimental error is considered, although it may be noted that the 1G model naturally yields poorer values of $F(h)$ because there are fewer parameters in the model than for the 2G or 5S models. Overall, however, it appears that the specific functional forms assumed in the electron density models are reasonable. Of course, from an electron density model, one also obtains predictions of $F(h)$ for higher values of h than can be observed. The predictions can be tested in two ways, (*a*) by comparing to the $h = 9$ and 10 TW data or (*b*) by the criterion that a large $F(h)$ for $h > 8$ would have been seen in our data but was not. The predictions shown in Table 1 satisfy the second criterion, although the 4S model (not shown) does not satisfy this criterion. None of the models satisfies the first criterion very well, and so some of the subsequent analysis will also utilize the TW data where the electron density models can be required to fit $F(9)$ and $F(10)$. As will be seen, the inclusion of $F(9)$ and $F(10)$ makes only small differences in the remainder of the results.

The main purpose of the electron density models is to obtain structural information. A typical set of structural results is shown in Table 2 for the 2G hybrid model. This table and how it is obtained will be explained in detail in subsequent paragraphs.

The first column of Table 2 gives the value of the scaling factor K by which the normalized structure factors in Table 1 were multiplied. The factor K is completely unknown from the data, which only yield relative values of $F(h)$. Given a value of K, all parameters of the electron density model are optimized except for the constrained value of $\rho^*_{CH_2}$ and the fluid electron density ρ^*_W.

TABLE 2 Calculated results ($H = 8$) for various structural quantities for the 2G hybrid model versus scaling factor K for $\rho^*_{CH_2} = 0.317$ e/Å^3

K	A	r	V_H	D_C	n_W	θ
e/Å^3	Å^2		Å^3	Å		*degrees*
2.54	51.9	1.95	339	15.5	16.9	40.0
2.60	49.8	1.94	339	16.2	14.7	37.0
2.66	47.9	1.93	340	16.8	12.7	33.9
2.72	46.0	1.92	340	17.5	10.7	30.3
2.78	44.4	1.91	341	18.1	9.0	26.6
2.84	42.9	1.90	341	18.7	7.4	22.1
2.90	41.5	1.89	342	19.3	5.9	16.6

From the fitted electron density model, $KF(0)$ is easily calculated according to its definition:

$$KF(0)/2 = \int_0^{D/2} [\rho^*(x) - \rho^*_W]dx \tag{6}$$

From the value of $KF(0)$ the area A is easily calculated from the first relation derived in the previous paper (22)

$$AKF(0)/2 = n^*_L - \rho^*_W V_L, \tag{7}$$

where n^*_L is the number of electrons in a lipid molecule, ρ^*_W is the electron density of the solvent, and V_L is the volume of the lipid molecule which is obtained from specific volume measurements (20, 21). Values of A are given in the second column of Table 2 which shows that A decreases roughly as $1/K$. (It may be noted that A decreases exactly as $1/K$ for unconstrained fits.)

The third column of Table 2 gives values of r, which is defined by $r = V_{CH_3}/V_{CH_2}$, where V_{CH_3} is the average volume of each terminal methyl and V_{CH_2} is the average volume of each methylene on the fatty acid chains. From the second recently derived relation (22)

$$V_{CH_3} = [n^*_{CH_3} + (AS_M/2)]/\rho^*_{CH_2}, \tag{8}$$

where $n^*_{CH_3}$ is the number of electrons in each methyl and S_M is half the integrated size of the central methyl trough in the electron density model. Table 2 shows that r is nearly constant as K is varied, which is consistent with Eq. (8) because A decreases roughly as $1/K$ and S_M increases roughly as K.

The fourth column in Table 2 gives the volume of the headgroup, V_H, which is obtained from V_L by subtracting the total volume, V_C, of the hydrocarbon region. V_C is the sum of the volumes of the methylenes (which are fixed in the constrained fits) and the volume of the terminal methyls which is proportional to r. Together this yields

$$V_H = V_L - V_C = V_L - n^*_{CH_2}[n_{CH_2} + rn_{CH_3}]/\rho^*_{CH_2}, \tag{9}$$

where n_{CH_2} and n_{CH_3} are the number of methylenes and methyls, respectively, in the fatty acid chains. Since the contribution of the methyls in Eq. 9 is small and the variation in r is small, V_C and V_H are nearly constant as a function of K.

The fifth column in Table 2 gives half the average thickness of the hydrocarbon region, defined by

$$D_C = V_C/A. \tag{10}$$

The hydrocarbon chain thickness D_C varies roughly as K. The sixth column in Table 2 gives n_W using Eq. 1. The seventh column gives the tilt angle θ using Eq. 2.

Results such as those illustrated in Table 2 have been generated for different values of $\rho^*_{CH_2}$ for the 1G and 2G hybrid models and for the 4S and 5S strip models defined in the Materials and Methods section. Examination of these results has revealed that the structural parameters can be functionally divided into two sets. Parameter set I consists of $\rho^*_{CH_2}$, r, and V_H. This parameter set is characterized by only small variations with K in either the constrained or unconstrained fits. The second parameter set consists of A, n_W, D_C, and θ. Parameter set II is characterized by strong variations with K. This division of the structural parameters into two nearly independent sets is most convenient for organizing the results of many calculations.

Our results for parameter set I are shown in Fig. 3 for six models for values of K which correspond to $\theta = 30°$ (e.g., $K \approx 2.72$ in Table 2 for the 2G model). If θ from parameter set II is changed to 35°, each of the lines in Fig. 3 shifts downward only by about one cubic angstrom, consistent with the aforementioned weak interdependence between the two parameter sets. The dashed lines in Fig. 3 show the lines of constant r which are obtained from Eq. 9. Given a model and a set of data, such as the 2G model, then any one of the three structural parameters, V_H, $\rho^*_{CH_2}$, and r, in parameter set I determines the other two using Fig. 3. The three models that contain two features in the headgroup region, namely the 2G, 2G (TW), and 5S models, agree well with each other in Fig. 3. Poorer agreement is obtained for the three models, 1G, 1G (TW), and 4S, that only contain one feature in the headgroup region.

Our results for parameter set II are shown in Fig. 4 for values of $\rho^*_{CH_2} = 0.317 \pm 0.003$ e/Å^3, the methylene density determined from wide-angle diffraction experiments. The use of parallel axes for A and n_W is justified by Eq. 1, which shows the simple and direct relation between these two structural parameters. The use of parallel axes for θ and D_C in Fig. 4 is justified because the variations in r are small enough that Eq. 10 combined with Eqs. 2 and 9 is effectively one between θ and D_C. The actual D_C scale shown in Fig. 4 is correct for the 2G model. The largest deviations are <0.1 Å for the 5S model and 2G (TW) models and <0.3 Å for the 1G, 4S, and 1G (TW) models. Variations of $\rho^*_{CH_2}$ by the experimental error of ±0.003 e/Å^3 shift the results to the lines on either side of the central results line in Fig. 4 which again demonstrates the weak interdependence between the two parameter sets. Therefore, given a physical range for the values of the structural parameters in parameter set I and the value of just one of the structural parameters in parameter set II, the other three structural parameters in set II are determined to good accuracy from Fig. 4.

DISCUSSION

The results in Fig. 3 show that the three models, 2G, 2G (TW), and 5S, with two features in the headgroup region agree very well with each other. This is encouraging from several points of view. First, the errors in the data and the

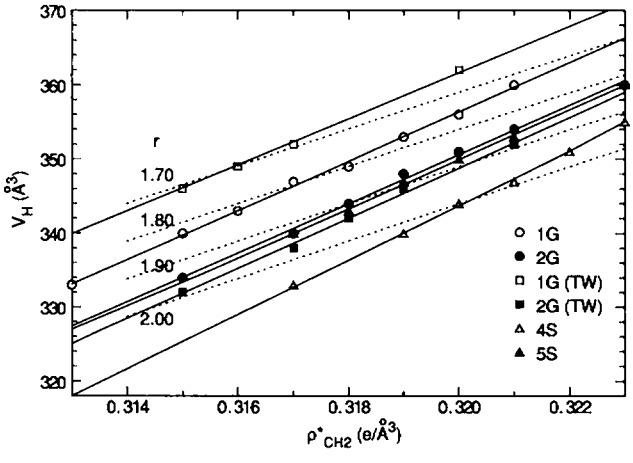

FIGURE 3 Parameter set I: Calculated results for six models for headgroup volume V_H versus methylene electron density $\rho^*_{CH_2}$. Loci of constant $r = V_{CH_3}/V_{CH_2}$ are shown by dashed lines with values of r indicated. All results are for tilt angle $\theta = 30°$. The lines passing through the results were obtained by linear least squares.

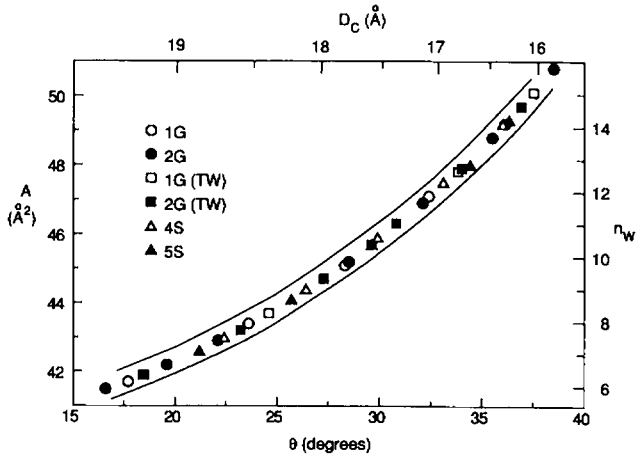

FIGURE 4 Parameter set II: Calculated results for area A (*left abscissa*), waters of hydration n_w (*right abscissa*), the chain tilt angle θ (*bottom ordinate*), and the hydrocarbon thickness D_C (*top ordinate*). Each of the results is for methylene electron density $\rho^*_{CH_2} = 0.317$ e/Å^3. The lines that bracket the data correspond to $\rho^*_{CH_2} = 0.314$ e/Å^3 (*upper line*) and 0.320 e/Å^3 (*lower line*).

necessary truncation of higher orders of diffraction do not seem to be important as seen by comparing the results of the hybrid 2G model obtained from the Torbet and Wilkins data with the results obtained from our data. Second, the precise functional form of the electron density model does not seem to affect the results as seen by comparing the results in Figs. 3 and 4 for the 2G hybrid model and the 5S strip model. The strip models have the sharpest conceivable boundaries and the hybrid models have very smooth boundaries. Agreement of results for these two disparate models would be supposed to extend to intermediate models, including the true bilayer electron density. The essential feature appears to be the capability of the model to accommodate an asymmetric headgroup by having two features in the headgroup region, either two Gaussians or two strips, as seen by comparing to the 1G and 4S models, which have only one feature in the headgroup region.

It had previously been clear that there is one relation, Eq. 9, between the three parameters, V_H, $\rho^*_{CH_2}$, and r, in parameter set I. What emerges from the modeling is a second relation which is the best line through the filled points in Fig. 3. Now, given any one of the three parameters, V_H, $\rho^*_{CH_2}$, and r, the other two can be determined. This is one of the main results of this work. However, it must be emphasized that one still requires "outside" information, i.e., information additional to the low-angle diffraction intensities and the specific volume, to determine all the parameters in parameter set I.

Using a value of the methylene electron density, $\rho^*_{CH_2} = 0.317 \pm 0.003$ e/Å^3, determined from the wide-angle diffraction experiments, a headgroup volume $V_H = 340 \pm 10$ Å^3 is obtained from Fig. 3. This range of values includes our earlier estimate of 348 Å^3, which from Fig. 3 requires values of $\rho^*_{CH_2}$ in the range 0.319 to 0.320 e/Å^3 which is also consistent with the values obtained from wide-angle diffraction. Also, the value obtained for the ratio r of terminal methyl volume to methylene volume is 1.93 ± 0.06, which is in the range of acceptable values considering that the gel phase of DPPC is somewhere between the fully crystalline chain systems, which have values of $r \sim 1.75$, and chain-disordered systems, which have values of $r \sim 2$ (19). In this connection, it may be noted that, while it is agreed that in the gel phase the chains are mostly all-*trans* in their central parts, there can be local disordering near the ends, which would tend to increase r for the terminal methyls to values closer to the chain-disordered values than to the crystalline values.

To determine the structural parameters, n_w, A, θ, and D_C, in parameter set II requires determining one of them, as is emphasized by Fig. 4. The only one that can be directly linked to the results of modeling the electron density profile is D_C. The idea is simply that D_C gives the boundary between the methylene region and the headgroup region, which can be visualized from the electron density profiles themselves. To examine the efficacy of this idea, consider the actual electron density profiles shown in Figs. 5 and 6 for the 1G, 4S, 2G, and 5S models. These particular profiles (which are, in fact, our best profiles) are for the models reported in Table 1, particularly for the K values given in Table 1 and $\rho^*_{CH_2} = 0.317$ e/Å^3. (The "best" 2G model derived from the TW data is shown in Fig. 1.) A solid line has been drawn in each profile corresponding to the value of D_C for that model calculated from Eq. 10. As K is decreased from the values given in Table 1 the calculated value of D_C decreases as can be seen in Table 2. The positions of the headgroup peaks and their widths stay roughly constant so that eventually such models would make the unreasonable prediction for small K that the hydrocarbon region ends at a point far from the headgroup peaks. The problem is how to define a precise and valid criterion for choosing D_C.

A simple and direct criterion to determine D_C is offered by the 4S strip model, namely the location of the discontinuity between the head and methylene regions (12). However, we believe this criterion should be viewed with caution. In particular, the definition of D_C must be clear, especially when comparing results from different studies. Our definition of D_C is the volume average position of the boundary between methylenes and headgroup. Since the two chains in DPPC are inequivalent (14) with the 1-chain connected to the glycerol group at a level smaller than D_C and the 2-chain connected at a level larger than D_C, D_C will not be the position at which the region of

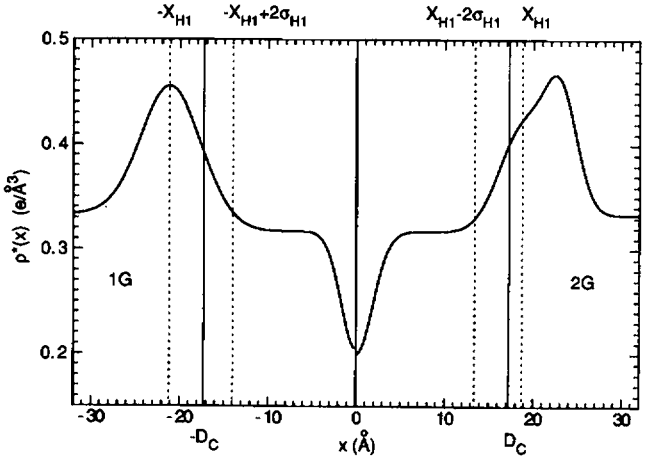

FIGURE 5 Absolute electron density profiles $\rho^*(x)$ as a function of distance x from the center of the bilayer obtained from the 1G model (*left*) and the 2G model (*right*). These profiles correspond to the values of K listed in Table 1. In each profile the calculated average boundary for the hydrocarbon region is represented by a solid vertical line designated $\pm D_C$. The center of the Gaussian, X_{H1}, is shown with a dotted labeled line, as is X_{H1}-$2\sigma_{H1}$.

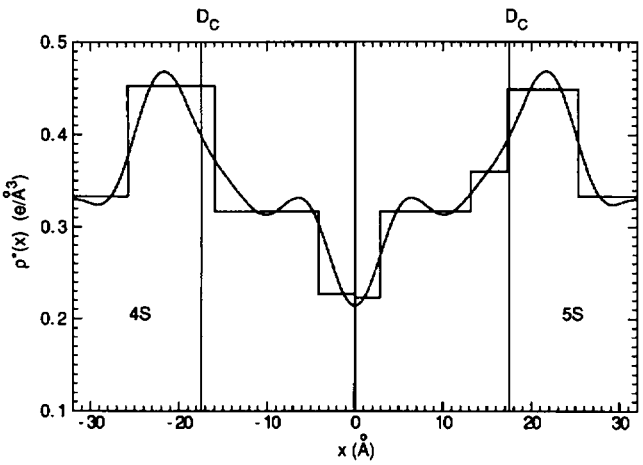

FIGURE 6 Absolute electron density profiles $\rho^*(x)$ as a function of distance x from the center of the bilayer obtained from the 4S model (*left*) and the 5S model (*right*). These profiles were generated using the values of K listed in Table 1. In each profile the calculated average boundary for the hydrocarbon region is represented by a solid vertical line designated $\pm D_C$. The Fourier series generated from the experimental data (Table 1) is also shown as a dashed line.

TABLE 3 Best values of average structural features of gel phase DPPC at T = 20°C with estimated uncertainties

D	63.7 ± 0.3 Å
D_C	17.5 ± 0.5 Å
D_W	13.9 ± 2.6 Å
D_H	7.4 ± 0.5 Å
D'_W	11.8 ± 0.8 Å
D'_H	8.5 ± 0.4 Å
D_B	49.8 ± 2.3 Å
$X_{H\text{-}H}$	45.0 ± 1.0 Å
A	45.9 ± 2.0 Å^2
$2A_C$	39.8 ± 0.4 Å^2
A'	40.0 ± 3.1 Å^2
V_L	1,144.0 ± 2.0 Å^3
V_X	1,462.0 ± 62.0 Å^3
V_C	804.0 ± 12.0 Å^3
V_H	340.0 ± 10.0 Å^3
V_{CH_2}	25.3 ± 0.2 Å^3
V_{CH_3}	48.8 ± 1.9 Å^3
θ	30.0 ± 3.0°
$F(0)$	0.388 ± 0.014
n_W	10.6 ± 2.0
n'_W	1.7 ± 1.5

constant methylene density ends. Rather, it should be closer to a position at which the carbonyl from the 1-chain increases the electron density above that of the constant methylene region. This is consistent with the values of D_C depicted in Figs. 5 and 6, which occur inside the headgroup strip and inside the headgroup Gaussians. We have also explored a number of other possibilities that will not be discussed here. Unfortunately, none allows us to exclude any value of D_C in the rough range form ~15 to ~19 Å based on the electron density profile criterion. From Fig. 4 one sees that this range yields fairly imprecise values of the other structural parameters in parameter set I.

From the preceding discussion it is appropriate to consider "outside" determinations for the parameters in parameter set II. It is our current view that the best outside value is $\theta = 30°$, which has been obtained to within 3° by three independent methods (10, 13, 14). Using this value of θ gives the K values shown in Table 1, the electron density profiles shown in Figs. 5 and 6, and the results shown in Table 3 for the other structural parameters in parameter set II.

It should be emphasized that the method used to obtain the results in the preceding paragraph is essentially the same as the method used in our previous paper (19). The results are, however, in disagreement because the experimental value $n_W = 13.6$ (3) was used there and the result $n_W = 10.6 \pm 2.0$ in this work follows from the measured values of θ. This highlights the fact that the literature values for θ are inconsistent with the more recent, higher values of $n_W = 17.5$ (2) and 19 (1), which were obtained by determining the hydration level at which the D spacing ceased to change. Instead the literature values of θ are more consistent with the n_W of 9 (7) obtained by hydrating from the vapor.

The conclusion of the preceding paragraph is surprising because the vapor hydration method produces significantly smaller D spacings than those obtained with fully hydrated lipid and this has properly weakened confidence in this method of obtaining n_W. We would like to suggest that the vapor hydration method gives results that are fortuitously close to our values due to the cancellation of two systematic errors, only one of which affects the D-spacing method. The basic assumption in thinking about n_W is that the bilayers are well-ordered in flat, parallel arrays with no imperfections. The idea that explains the above anomalous results is to allow for imperfections, such as those that must occur in the centers of liposomes or where liposomes impinge upon one another. In the fully hydrated state such regions will likely have a larger water/lipid ratio compared to the perfectly oriented system. These imperfections would make n_W appear larger in the D-spacing method of measuring n_W. Such imperfections would, however, have relatively little effect upon the lamellar diffraction which is used in our analysis because the diffraction preferentially focuses on the more perfect regions. It is, therefore, not proper to mix the n_W results obtained using the D-spacing method with our results. Furthermore, the value of n_W is less fundamental that ours since it depends upon the extent of imperfections which in turn depends upon the degree of

annealing of the system and is subject to large fluctuations as the literature indicates. The method of hydrating from the vapor is also subject to this systematic error as well as to the error that the lipid never becomes fully hydrated. We suggest, therefore, that n_W may only be obtainable indirectly, as in this paper.

Our value of $F(0)$, 0.388 ± 0.014, was obtained by averaging the three values for the 2G, 2G (TW), and 5S models given in Table 1. It differs significantly from two previously quoted values, 0.86 from Torbet and Wilkins (9) and 0.25 from McIntosh and Simon (11). The result of Torbet and Wilkins was estimated from examining molecular models of DPPC and those authors acknowledged that the value of $F(0)$ was strongly dependent upon the particular model used. The primary thrust of their paper, the determination of the higher order phases of the lamellar reflections, did not depend critically upon $F(0)$, implying that they did not attach much weight to their particular value of $F(0)$. McIntosh and Simon utilized five orders of diffraction obtained at different levels of hydration in their estimate of $F(0)$. With only five orders of diffraction, $F(0)$ is not very well-determined (Nagle, J. F., unpublished calculations), and like Torbet and Wilkins (9), McIntosh and Simon did not attach much weight to their particular value. In our opinion the use of constrained electron density models is the best method for the determination of $F(0)$. Using our value of $F(0)$, the absolute continuous transform $F(X)$ was constructed using the sampling theorem (9, 18) and is shown in Fig. 7.

One of the most quoted results from low angle x-ray studies is the distance between the headgroups, $X_{H\text{-}H}$, which is often associated with the phosphate–phosphate distance, which is a measure of the bilayer thickness. Results for $X_{H\text{-}H}$ may be obtained from Fig. 8, which focuses on the peak of the headgroup region. The 2G model (with $H = 8$) and the 2G (TW) model (with $H = 10$) both yield $X_{H\text{-}H}$ near 45 Å. The Fourier series with $H = 6$ has a peak near 42 Å, the Fourier series with $H = 8$ has a peak closer to 43 Å, whereas the peak of the $H = 10$ Fourier series is a little greater than 44 Å. It appears that the Fourier series tend to underestimate $X_{H\text{-}H}$ for finite H. Furthermore, the peak of the total electron density is located closer to the center of the bilayer than the peak in the outer Gaussian. Thus, if one supposes that the phosphate is located at the center of the outer feature, the phosphate–phopshate distance is further underestimated from finite H Fouriers. However, the total underestimation is <4 Å for $H = 6$.

Table 3 collects all the data and the results for parameter sets I and II, $F(0)$, and $X_{H\text{-}H}$. It also gives results for many additional structural parameters which have been carefully defined elsewhere (19). As noted in (19), it is unrealistic to constrain the mean area of the headgroup to

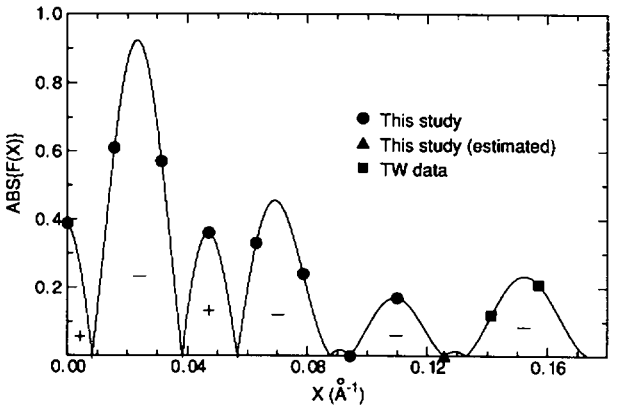

FIGURE 7 Continuous scattering transform $F(X)$ of gel phase DPPC. $F(h)$ for $h = 0$ to 8 are from column 2 in Table 1 and $F(9)$ and $F(10)$ are from column 4 in Table 1. For absolute values multiply by the K values in the last column of Table 1. The phases of the various regions are indicated by the + and − signs on the figure.

be the same as the area A per molecule (even though some sections through the headgroup probably achieve this area). It is appropriate to represent the mean size of the headgroup by area A' and thickness D'_H. This allows n'_W of the n_W water molecules to enter the headgroup region and the thickness of the pure water region becomes D'_W (so that $2D_C + 2D'_H + D'_W = D$). Earlier estimates of these primed (') quantities required a value of D'_H, which was crudely estimated from the neutron diffraction studies of Buldt et al. (14) to be 8 Å, our estimate (19), or 9 Å (15). The results of electron density modeling allow a different procedure for the determination of D'_H. The boundary of the hydrocarbon region, extending to $D_C \approx 17.5$ Å, is

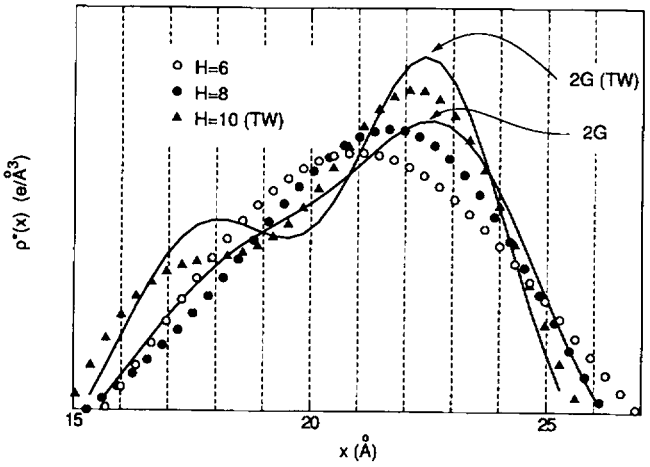

FIGURE 8 Electron densities for the 2G model ($H = 8$), the 2G (TW) model ($H = 10$), and the $H = 6$, 8, and 10 Fourier series in the headgroup region versus distance x from the center of the bilayer.

taken to represent one side of the headgroup region. For the other boundary between the headgroup and the interlamellar water $X_{H2} + 2\sigma_{H2}$ may be consistent at which $\rho^*(x) \approx \rho_W^*$. This leads to a vlaue of $D'_H = 8.5$ Å. Also, a value of $D'_W = 11.9 \pm 0.8$ Å is obtained from a consideration of the 2G, 5S, and 2G (TW) models. These values compare well with the result of 11.5 Å given by McIntosh and Simon (11) for the thickness of the interlamellar water layer between fully hydrated G phase DPPC bilayers.

CONCLUSIONS

A unified method to analyze volumetric and diffraction data in the determination of the structure of fully hydrated bilayers has been demonstrated. In particular, the low-angle intensity data have now been fully integrated into our previous analysis (19). This analysis has the flexibility of choosing the more certain of the experimentally determined quantities and in checking the consistency of various data (see Fig. 4 for example).

While electron density modeling has been pursued for some years, the derivation (22) and use of relations for obtaining structural information in addition to the parameters of the particular density function fit to the data is a new result. In addition the hybrid models developed here are continuous electron density functions that provide an appealing representation of the bilayer. (See Figs. 1, 5, and 6.) In particular, the Gaussian representation of the headgroup and terminal methyl regions yields profiles more similar in appearance to the Fourier series electron density profiles than the simple strip models. However, an important result is that the smooth hybrid model yields the same structural results as the sharply discontinuous strip model (see Figs. 3 and 4) provided that two features are included in the headgroup region for each model. Therefore, the results of the analysis are not sensitive to guessing precisely the unknown functional form for the electron density of the bilayer.

When applied to either our data or the data of Torbet and Wilkins (Table 2 and Fig. 2), our analysis yields consistent results for a large number of structural parameters characterizing bilayers in the fully hydrated gel phase of DPPC as shown in Table 3. The only additional datum used in the analysis was the value of the tilt angle θ measured by others (10, 13, 14).

Received for publication 15 June 1988 and in final form 17 October 1988.

REFERENCES

1. Ruocco, M. J., and G. G. Shipley. 1982. Characterization of the sub-transition of hydrated dipalmitoylphosphatidylcholine bilayers: kinetic, hydration and structural study. *Biochim. Biophys. Acta.* 691:309–320.
2. Lis, L. J., M. McAlister, N. Fuller, R. P. Rand, and V. A. Parsegian. 1982. Interactions between neutral phospholipid bilayer membranes. *Biophys. J.* 37:657–666.
3. Janiak, M. J., D. M. Small, and G. G. Shipley. 1976. Nature of the thermal pretransition of synthetic phospholipids: dimyristoyl- and dipalmitoyllecithin. *Biochemistry.* 15:4575–4580.
4. Tardieu, A., V. Luzzati, and F. C. Reman. 1973. Structure and polymorphism of the hydrocarbon chains of lipids. *J. Mol. Biol.* 75:711–733.
5. Inoko, Y., and T. Mitsui. 1978. Structural parameters of dipalmitoyl phosphatidylcholine lamellar phases and bilayer phase transitions. *J. Phys. Soc. Jpn.* 44:1918–1924.
6. Luzzati, V. 1967. X-ray diffraction studies of lipid-water systems. *In* Biological Membranes. D. Chapman, editor. Academic Press, London. 71–123.
7. Jendrasiak, G. L., and J. H. Hasty. 1974. The hydration of phospholipids. *Biochim. Biophys. Acta.* 337:79–91.
8. Mitsui, T. 1978. X-ray diffraction studies of membranes. *Adv. Biophys.* 10:97–135.
9. Torbet, J., and M. H. F. Wilkins. 1976. X-ray diffraction studies of lecithin bilayers. *J. Theor. Biol.* 62:447–458.
10. McIntosh, T. J. 1980. Differences in hydrocarbon chain tilt between hydrated phosphatidylethanolamine and phosphatidylcholine bilayers. *Biophys. J.* 29:237–245.
11. McIntosh, T. J., and S. A. Simon. 1986. Hydration force and bilayer deformation: a reevaluation. *Biochemistry.* 25:4058–4066.
12. King, G. I., and S. H. White. 1986. Determining bilayer hydrocarbon thickness from neutron diffraction measurements using strip-function models. *Biophys. J.* 49:1047–1054.
13. Levine, Y. K. 1973. X-ray diffraction studies of membranes. *Prog. Surf. Sci.* 3:279–352.
14. Buldt, G., H. U. Gally, A. Seelig, J. Seelig, and G. Zaccai. 1978. Neutron diffraction studies on selectively deuterated phospholipid bilayers. *Nature (Lond.).* 271:182–184.
15. McIntosh, T. J., and S. A. Simon. 1986. Area per molecule and distribution of water in fully hydrated dilauroylphosphatidylethanolamine bilayers. *Biochemistry.* 25:4948–4952.
16. Worthington, C. R. 1969. The interpretation of low-angle X-ray data from planar and concentric multilayered structures: the use of one-dimensional electron density strip models. *Biophys. J.* 9:222–234.
17. Worthington, C. R., and A. E. Blaurock. 1969. The structural analysis of nerve myelin. *Biophys. J.* 7:970–990.
18. Worthington, C. R., G. I. King, and T. J. McIntosh. 1973. Direct structure determination of multilayered membrane-type systems which contain fluid layers. *Biophys. J.* 13:480–494.
19. Nagle, J. F., and M. C. Wiener. 1988. Structure of fully hydrated lipid dispersions. *Biochim. Biophys. Acta.* 942:1–10.
20. Nagle, J. F., and D. A. Wilkinson, 1978. Lecithin bilayers: density measurements and molecular interactions. *Biophys. J.* 23:159–175.

21. Wiener, M. C., S. Tristram-Nagle, D. A. Wilkinson, L. E. Campbell, and J. F. Nagle. 1988. Specific volumes of lipids in fully hydrated bilayer dispersions. *Biochim. Biophys. Acta.* 938:135–142.

22. Nagle, J. F., and M. C. Wiener. 1989. Relations for lipid bilayers: connection of electron density profiles to other structural quantities. *Biophys. J.* 55:309–313.

23. Wiener, M. C. 1988. Specific Volumes and Structure of Fully Hydrated Phospholipid Bilayers. Ph.D. Thesis. Carnegie Mellon University, Pittsburgh, PA.